International Journal of Fatigue 65 (2014) 78–85

Contents lists available at ScienceDirect

International Journal of Fatigue

journal homepage: www.elsevier.com/locate/ijfatigue

Short fatigue crack propagation during low-cycle, high cycle and very-high-cycle fatigue of duplex steel – An unified approach

Ulrich Krupp [a,*], Iris Alvarez-Armas [b]

[a] Faculty of Engineering and Computer Science, University of Applied Sciences, 49009 Osnabrück, Germany
[b] Instituto de Física Rosario – CONICET, Universidad Nacional de Rosario, Bv. 27 de Febrero 210bis, 2000 Rosario, Argentina

ARTICLE INFO

Article history:
Received 20 February 2013
Received in revised form 10 June 2013
Accepted 18 June 2013
Available online 19 July 2013

Keywords:
Duplex steel
Short fatigue cracks
LCF
VHCF
Modeling

ABSTRACT

The present paper reviews experimental results on the fatigue damage of austenitic–ferritic duplex steel under various load levels ranging from LCF to VHCF, placing the focus towards the relationship between the crystallographic orientation of individual grains and grain patches that exhibit slip band formation, fatigue crack initiation and growth. A combination between fatigue testing of electropolished specimens and analytical electron microscopy (SEM/EBSD, TEM) revealed that under LCF loading conditions almost all the ferrite and the austenite grains showed plasticity, while under HCF and VHCF loading conditions, slip band formation was limited to the softer austenite grains and a low plastic activity is observed in the ferrite. Once being formed, the bands generate high stress concentrations, where they impinge the α–γ phase boundaries, eventually, leading to the crack initiation. This is discussed by applying a numerical simulation approach based on the finite-element (FEM) and the boundary-element (BEM) method.

1. Introduction

Duplex stainless steels (DSS) are increasingly used for industrial applications that involve fatigue loading in corrosive environments. Due to the high Cr and Mo content DSS exhibit a superior resistance to stress-corrosion cracking. The mechanical properties can be tailored for the two phases, bcc ferrite (α) and fcc austenite (γ), separately by heat treatment (475 °C embrittlement) or nitrogen alloying [1].

Fatigue damage generally initiates at plastic strain concentration sites. Under low-cycle fatigue (LCF) loading conditions, plastic deformation involves large areas of a structure and causes immediate multiple-site crack initiation. Previous studies in the LCF regime have revealed that when the material is in the as-received form, all the ferrite and the austenite grains showed plastic deformation [2].

The lower critical shear stress and the planar slip character of the dislocations produce a homogeneous slip band distribution earlier in the austenite than in the ferrite. The associated dislocation structure belongs to dislocation bands on one or two {1 1 1} slip planes. In the ferrite, dislocations present the typical wavy slip character and the slip markings in the specimen surface are composed of all kind of slip features, i.e., slip lines, band-like extrusions, curvilinear cord-like extrusion and highly rugged areas. Strain localizes in these rugged zones, which promote crack initiation [3,4]. According to other authors, microcracks may nucleate in an intergranular manner in the ferrite areas, which is in agreement with the analysis of Vogt et al. [4], or along persistent slip bands in those grains where single slip is more favourable. Microcracks propagate in an oscillating way until their coalescence [5,6]. In particular in the case of high mean stresses, crack coalescence strongly contributes to short crack propagation, which can be attributed to a high crack density (cf. [7]). Finally, a large portion of the fatigue life is determined by long fatigue crack propagation (technical cracks, cf. Fig. 1a), which can be assessed by, e.g., the empirical Paris law (for an overview see [8]).

Contrary to that, high-cycle (HCF) and very-high-cycle fatigue (VHCF) damage occurs locally, when the applied load is macroscopically elastic. Second phases of different mechanical properties as well as crystallographically misoriented grains give raise to stress concentration that leads to the development and growth of slip bands during cycling [9,10]. These bands may be blocked by or transmitted through grain and phase boundaries. Due to partial irreversibility of cyclic plasticity along single slip bands (cf. Section 4), vacancy-type annihilation of dislocations moving back and forth at the slip band can be considered as infinitesimal crack advance. Arrest and overcoming grain and phase boundaries by the plastic zone and the crack, respectively, give rise to an oscillating fatigue crack propagation rate. In the case of VHCF, this oscillation may prevail throughout the complete fatigue life [10,11]. If the microstructural barriers are strong enough, all the initiated cracks

* Corresponding author. Tel.: +49 541 9692188; fax: +49 541 9697047.
E-mail address: u.krupp@hs-osnabrueck.de (U. Krupp).

0142-1123/$ - see front matter © 2013 Elsevier Ltd. All rights reserved.
http://dx.doi.org/10.1016/j.ijfatigue.2013.06.018

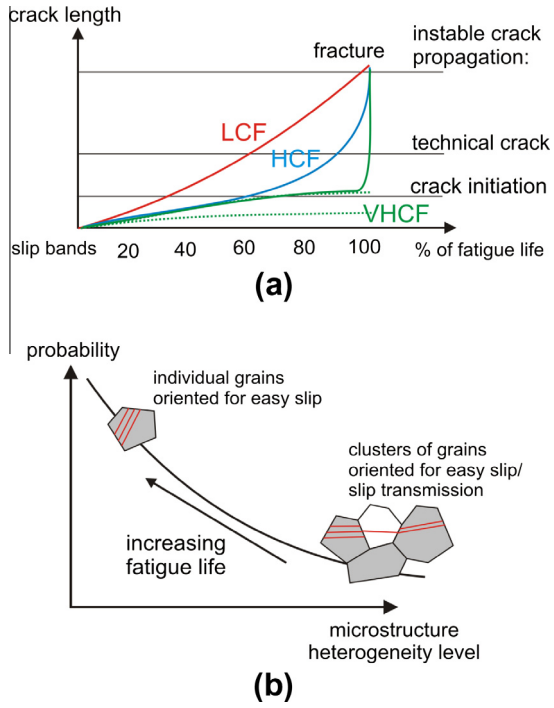

Fig. 1. Schematic representation of (a) the damage development (crack length) during LCF, HCF and VHCF, and (b) the probability of the occurrence of microstructure heterogeneities as a function of the heterogeneity level (cf. [12]).

are blocked, and the fatigue limit is reached. Accordingly, the resistance to fatigue damage for low stress amplitudes (HCF and VHCF) becomes strongly dependent on the microstructure heterogeneity level and the probability of the occurrence of critical heterogeneities [12], the latter being dependent on the specimen or component size and the production process, respectively. This is shown schematically in Fig. 1b. In the case of duplex steel, the response to fatigue loading depends on the initial mechanical conditions (stress or strain range, strain rate, etc.) and on the mechanical strength of the two phases [1,8,13]. In earlier work it was found that cyclic plasticity is partitioned mainly to the softer austenite phase leading to the occurrence of elastic residual stresses in the ferrite grains during HCF and VHCF or the mutual interaction of the phases to accommodate plastic deformation during LCF. Therefore, slip bands and microstructural crack formation cause stress relief and the onset of the fatigue damage process.

The present paper summarizes previous results on HCF and VHCF in the homogenized DSS and adds new results of LCF and HCF experiments varying the strength of the ferritic phase by an embrittlement heat treatment. As well, it will be outlined how the apparently different damage mechanisms can be assessed by a uniform short crack modelling concept.

2. Experimental

The duplex stainless steel used in this study, with the chemical composition according to Table 1, was given a grain-coarsening heat treatment in order to ease 2D and 3D measurements of the crystallographic orientation distribution. The strength of the ferrite phase was varied by means of an embrittlement heat treatment causing the formation of Cr-rich α' precipitates within the ferrite grains by spinodal decomposition [1]. The heat treatment parameters and the corresponding yield stress, hardness and grain-size values are represented in Table 1.

The two-phase microstructure (phase fractions about 50% α and γ, resp.) is shown in Fig. 2a, in a cross section normal to the rolling direction. Mechanical testing was carried out on various mechanical conditions in a wide fatigue range. HCF and VHCF tests were performed in resonant fatigue testing (RUMUL Testtronic, 40–260 Hz), servohydraulic (MTS 810, 1000 Hz) and ultrasonic (BOKU 20 kHz) testing systems using different specimen geometries, mainly under stress control and a stress ratio of $R = -1$. Fig. 2b and c show the shallow-notched specimen design that allows limitation of crack formation within an electropolished notch area (notch factor $\beta \approx 1.1$). In-situ observations with a long-distance QUESTAR optical microscope coupled to a digital camera at the testing machine were made. As well, a discontinuous evaluation of fatigue damage at the surface by scanning electron microscopy in combination with automated electron back scatter diffraction (EBSD) were carried out [14,15]. For LCF tests an electromechanical Instron machine mod.1362 was used. Testing was performed under plastic-strain control with a fully reversed triangular wave at total strain rate of $2 \times 0^{-3}\ s^{-1}$. In order to characterize the surface damage, the test was stopped (at 80% of σ_{Max}) periodically. Fig. 2c shows the shallow-notched specimen design that allows crack initiation in a limited electropolished area. The flat part of the notch for LCF was systematically explored during the test using a high resolution CCD camera JAI mod. CM-140MCL with a 50× objective and a 12× ultra zoom device mounted on the fatigue test machine.

3. Results

During LCF in the embrittled condition, the austenite phase presents – as in the as-received condition – homogeneous distribution of planar slip markings, while the ferrite exhibits first straight slip lines, which turn into slip bands during ongoing cycling. One characteristic feature of these bands is that they are heterogeneously distributed on the specimen surface as is illustrated in Fig. 3a and b. In fact, the ferrite presents planar slip- or less wavy slip-character due to spinodal decomposition; dislocations are more confined to their glide planes not being able to cross slip as usually occurs in a bcc structure [16]. This fact was proven in earlier papers by Gironés et al. and Armas et al. [17,18]. During fatigue, the back and forth dislocation motion diminishes the amplitude of the spinodal decomposition [19], which favours the subsequent dislocation motion and the generation of localized deformation regions

Table 1
Chemical composition (in wt%) and heat treatment parameters of the duplex steel (German designation 1.4462) used in this study.

Fe	C	Cr	Ni	Mo	Mn	N	P	S
Bal.	0.02	21.9	5.6	3.1	1.8	0.19	0.023	0.002

Homogenized condition + grain coarsening	1250 °C (4 h), followed by slow cooling to 1050 °C and, eventually, water quenching Ferrite: grain size 33 μm, hardness 280 HV Austenite: grain size 46 μm, hardness 260 HV Yield stress: 550 MPa
Embrittled condition + grain coarsening	1250 °C (4 h) followed by slow cooling to 1050 °C and, eventually, water quenching 475 °C (100 h) Ferrite hardness 465 HV Yield stress: 830 MPa

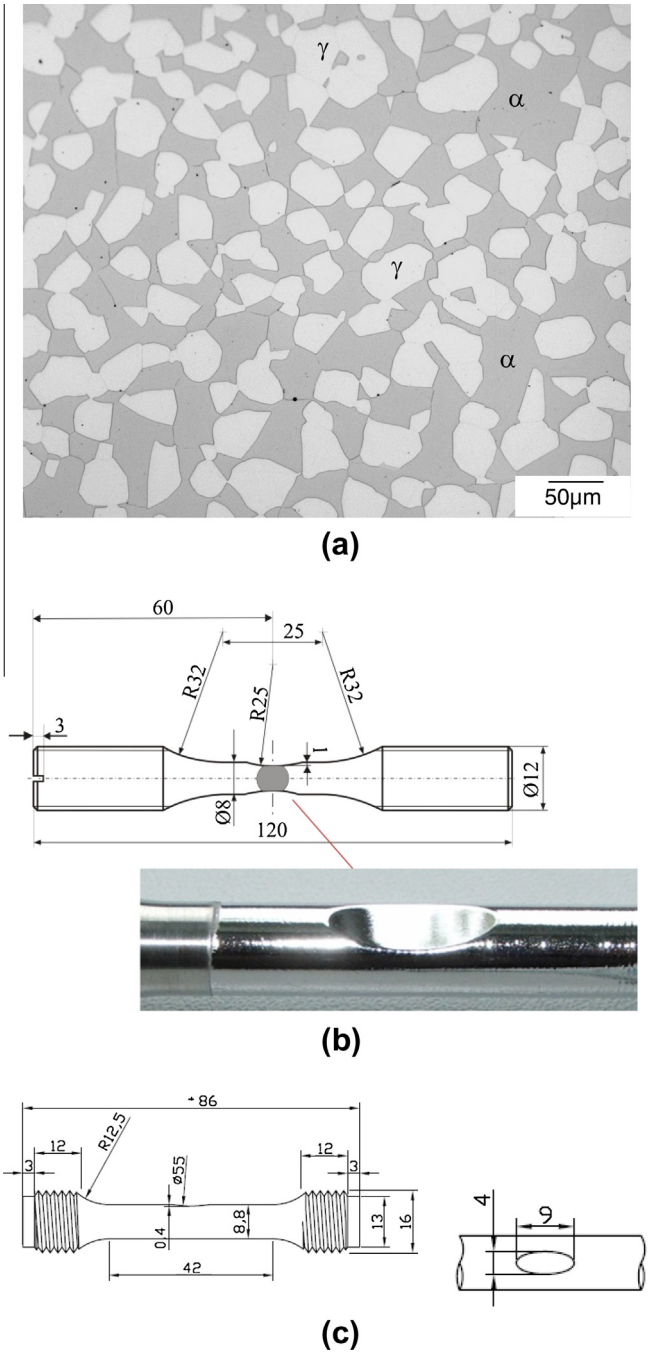

Fig. 2. (a) Ferritic–austenitic microstructure of the duplex steel used in this study, (b) specimen geometry for HCF and VHCF, and (c) LCF testing.

(microbands), Fig 3c and d. This deformation concentrates in bands along the {1 1 0} and {1 1 2} planes, which lastly give rise to the formation of microcracks when these planes intersect the free surface of the specimen [15,20]. Alternatively, the critical strain concentrations at the intersection of these bands to the phase-boundary can form crack nuclei as well, Fig. 3d. Microcrack grows in an oscillating way, being the α–γ phase boundary a barrier to crack propagation. The strength of this barrier depends on the crystallographic misorientation angles between neighbour grains [13].

Under HCF in the homogenized DSS, the cyclic plastic activity begins after few cycles in the austenitic phase. As cycling proceeds, slip lines intensify and finally most of them propagate into the ferrite. The concentration of stresses in the ferrite increases and slip markings intensify and turn into coarse bands that can remain arrested at the grain boundary, Fig. 4a. TEM micrographs show a certain degree of plastic activity in the ferrite not forming complex structures, Fig. 4b. In the embrittled DSS, the first slip markings appear mostly in the austenitic phase and as cycling proceeds, these lines intensify and some propagate into the neighbouring ferritic grains or remain arrested at boundaries. Microcracks often nucleate mostly at α–γ boundaries and then propagate along slip markings formed successively in the austenitic and ferritic grains, Fig. 4c and d. To a less extent, microcracks can also nucleate on slip markings in the austenite and at α–α boundaries [21].

VHCF loading conditions were tested only in the homogenized DSS. The plastic activity seems to be limited to the softer austenite grains. This kind of plasticity, occurring at a remote stress amplitude below the macroscopic yield strength, can be attributed to the elastic anisotropy of the material, which has been proven by the finite element simulations (cf. Section 4). In accordance to earlier work of Heinz and Neumann [22] and Blochwitz and Tirschler [23], twin boundaries were found to be preferential slip-band initiation sites. Once being formed, the bands generate high residual stress concentrations at the α–γ phase boundaries, Fig. 5a and b, eventually leading to the formation of isolated slip bands in the ferrite, which are enclosed in dotted lines on Fig. 5a. Actually, fatigue damage in the VHCF regime causes the formation of slip bands followed by initiation and propagation of microstructurally cracks in a pronounced localized manner, manifesting itself by heat generation [10,24]. Accordingly, under VHCF conditions, slip activity was found to occur at low stress amplitudes ($N > 10^8$ cycles) without fracture.

It is clear that with decreasing plastic strain/stress amplitude, the number of grains exhibiting slip bands decreases. It was shown that the number of slip bands in those grains increases with increasing number of cycles due to cyclic irreversibility and work hardening on the individual slip planes. At the same time, back and forth dislocation movement on separate slip planes of the same band during cycling leads to vacancy-type annihilation [25,26]. Eventually, this mechanism results in crack formation and propagation along a slip band.

In the case of the austeno-ferritic stainless steel, once a microcrack is nucleated (microstructural short crack), the propagation is in an oscillating way until the macro-crack sets in. This behaviour can be rationalized due to the following facts:

(i) The growth process in the softer austenite is much slower than in the ferrite due to the activation of alternating slip systems, while the propagation in the ferrite is rather fast and even faster in the embrittled phase. The propagation path of microstructural cracks in the ferrite seems to follow single slip markings (band-like extrusions).
(ii) A high misorientation angle between the slip systems in the neighbouring grains (subdivided in twist and tilt angle with respect to the grain-boundary plane) was correlated with a strong barrier effect, i.e., the crack propagation decreases.

Therefore, HCF and LCF is governed by the same relationship between the misorientation between neighbouring grain or phase areas and the oscillating propagation behaviour of microstructurally short fatigue cracks in both the homogenized and the embrittled DSS. These elements were used to simulate the early fatigue crack propagation process in HCF in earlier papers [14,21,27]. Likewise, the simulation of the fatigue crack propagation was proven in the present paper using previous results [13,15,28] and adapting the existing parameters [8,29,30] for the LCF regime (cf. Section 4).

Fig. 6a and b shows the fatigue life under LCF and HCF/VHCF loading conditions in the homogenized and embrittled DSS, respectively [10,31]. They clearly show an increment of the fatigue life in

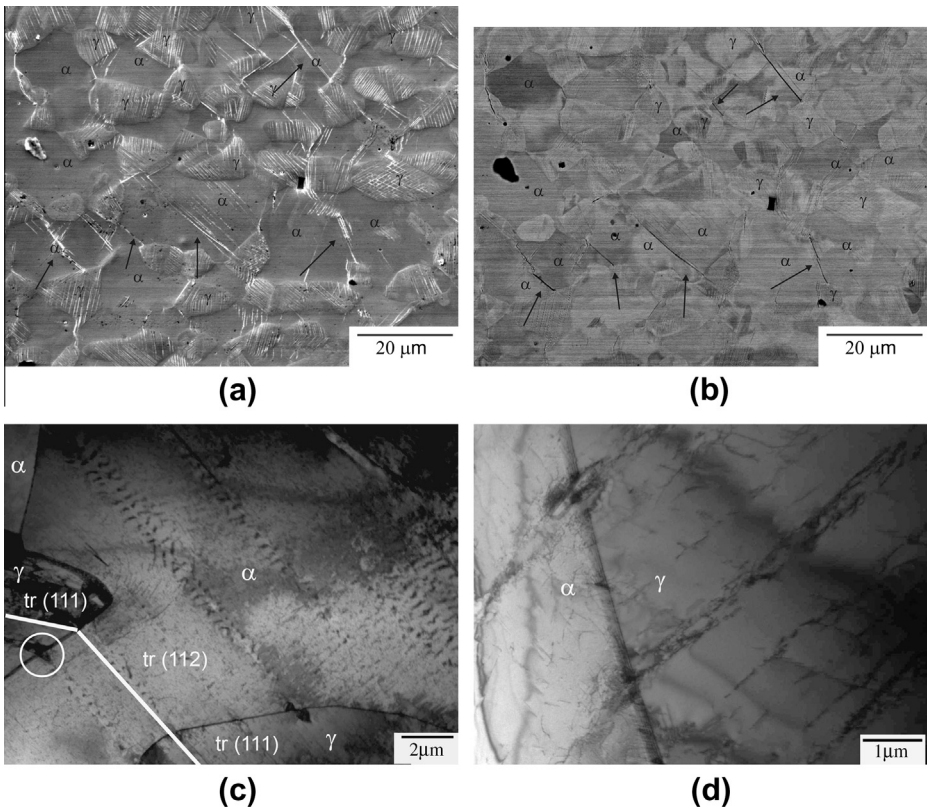

Fig. 3. LCF-loaded specimen: $\Delta\varepsilon_p = 0.3\%$ (a) secondary electrons (SE) contrast showing slip bands in the austenite phase and (b) back-scattered electrons (BSE) contrast showing microcracks in the ferrite phase [15], $\Delta\varepsilon_p = 0.3\%$ (c and d) TEM dislocation structure: localized deformation regions (microbands) along glide planes in the ferrite phase. (d) This image gives evidence of the strain propagation between phases through the phase boundary.

the embrittled condition under HCF and VHCF. Recent experiments using ultrasonic fatigue at 20 kHz have shown that even at 10^9 cycles the aforementioned damage process is active: slip band formation in the austenite grains in combination with an increase of the (elastic) residual stresses in the ferrite grains. Under LCF conditions, the embrittled condition slightly decreases the fatigue life rather than worsen it drastically. Actually, the different stages from strain localization along slip bands (microbands formation) up to the corresponding crack nuclei formation is a gradual process and rather comparable with the process of strain localization (persistent slip band PSB formation) in the homogenized DSS [6].

The barrier efficiency of grain and phase boundaries was estimated by evaluating cyclic stress strain curves (cyclic yield strength σ_{cY}) of fcc, bcc and duplex steel with various grain sizes d according to the Hall–Petch approach (for details see [11]). Here, the critical shear stress for slip was set equal to the (cyclic) friction stress τ_{fr} in Eq. (1) and the barrier strength were derived from the cyclic Hall–Petch constant k_c (Table 2).

$$\frac{\sigma_{cY}}{2} = \tau_{fr} + k_c \frac{1}{\sqrt{d}}. \tag{1}$$

This was done for the individual phases as well as for grain and phase boundaries to obtain the required data set for simulation of the early fatigue crack propagation process in DSS.

4. Discussion and modelling concept

For microstructure-based modelling of LCF, HCF and VHCF damage of DSS, the grain and phase distribution with the respective crystallographic orientations, the critical shear stress (friction stress τ_{fr}) to activate plastic slip, and the barrier strength of phase and grain boundaries need to be known. EBSD measurements of surface areas, where slip bands and/or microcracks were found, allow the reproduction of the respective microstructure as a FE mesh (2D plate with 8 elements thickness). By knowing the direction-dependent values of the stiffness tensor (elastic anisotropy) and the directions of the slip systems of the grains involved, locations of plastic strain concentration were predicted. These locations were correlated with the slip band and/or crack initiation sites (see Fig. 7).

Once the crack initiation sites are known, the number of cycles to crack initiation N_i is the second question to be answered. Tanaka and Mura [25] and later Chan [26] suggest a concept, which is based on dislocation dipole accumulation on slip bands and dislocation pile up at the grain boundaries with the respective grain size d. Here, the difference between the shear stress amplitude $\Delta\tau$ applied on the respective slip plane and the value of the friction stress τ_{fr} acts as driving force for the crack initiation process.

$$N_i \approx \frac{4Gw_s}{\pi(1-\nu)d(\Delta\tau - 2\tau_{fr})^2}. \tag{2}$$

While the original model of Tanaka and Mura is based on the specific fracture surface energy w_s, Chan extended the model taking the slip band width h and an irreversibility factor for cyclic slip λ into account. Then, the number of cycles N_i for initiation of a crack of length a can be calculated as:

$$N_i \approx \frac{8G^2}{\lambda\pi(1-\nu)}\left(\frac{a}{d}\right)\left(\frac{h}{d}\right)^2 \frac{1}{(\Delta\tau - 2\tau_{fr})^2}, \tag{3}$$

with G being the shear modulus and ν the Poisson ratio.

Once a crack has nucleated, it is assumed to propagate along slip bands. This process has been assessed by a boundary-element

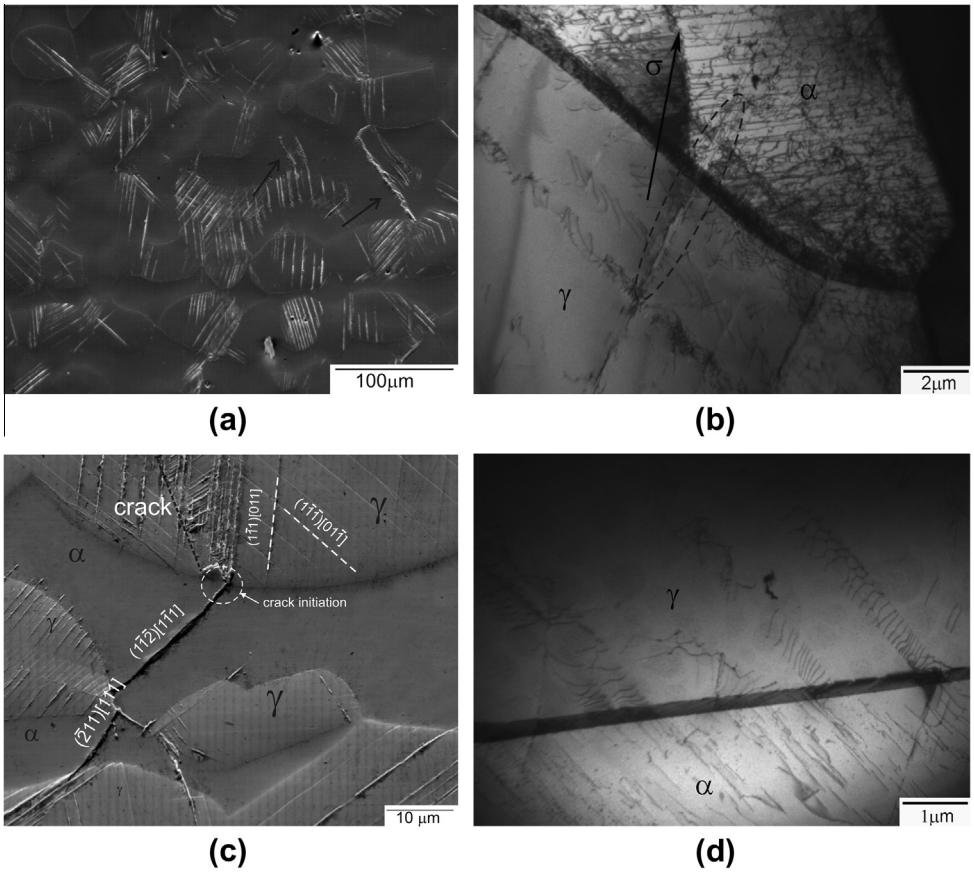

Fig. 4. HCF-loaded specimen: $\Delta\sigma/2 = 350$ MPa; $R = -1$. Homogenized DSS: (a) SEM micrograph showing slip lines in both phases, (b) TEM micrograph showing the intense slip activity in the ferrite, (c) SEM micrograph showing the crack initiation at phase boundary and the crack path after fatigue, and (d) stress concentration zones due to pile-ups of dislocations at grain boundary.

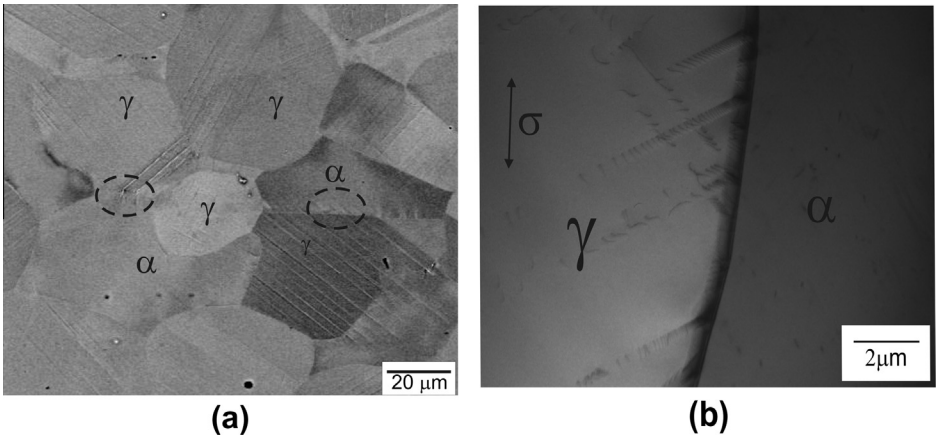

Fig. 5. VHCF loading of homogenized DSS specimens $\Delta\sigma/2 = 300$ MPa; $R = -1$: (a) SEM micrograph showing intense slip marking in the austenite bands and some of them generate high residual stress concentrations at the (γ–α) phase boundaries; and (b) dislocation pile-ups at a (γ–α) phase boundary.

(BEM) approach [8,29,30], where the crack and the adjacent slip bands are meshed by boundary elements that represent tangential displacement steps within the slip band and tangential/normal displacement steps within the crack area. These displacement steps can be considered as mathematical dislocation dipoles. Therefore, the interaction between two elements i and j can be calculated on the basis of stress fields around edge dislocations. For all slip-band and crack elements an equation system can be setup and solved accounting for the boundary conditions that (i) the normal stresses within the crack must be positive, (ii) no shear stresses appear in the crack area, and (iii) the shear stresses within the plastic zone are limited by τ_{fr}. Solution of the equation system provides the displacement field along the crack and the yield strips (slip bands) in front. The displacement at the crack tip, i.e., displacement interval between maximum and minimum load $\Delta CTSD$ is used as crack driving force, using the following crack propagation law:

$$\frac{da}{dN} = C \cdot \Delta CTSD, \tag{4}$$

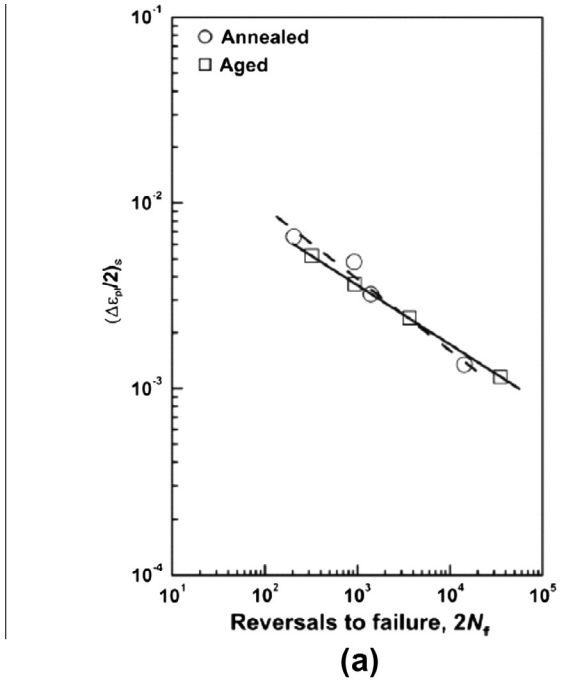

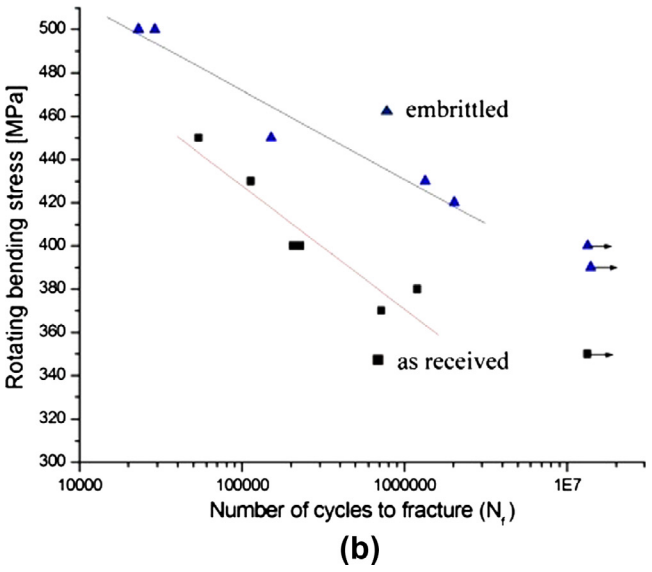

Fig. 6. Fatigue life of homogenized and embrittled DSS: (a) LCF data and (b) HCF data.

with C being a constant representing the irreversible fraction of crack-tip displacement having a similar meaning than the constant λ used in Eq. (1). The constant C was adapted to the experimental results yielding $C = 0.002$, which was used for all simulations in the embrittled steel during HCF, and $C = 0.08$ for LCF. It has to be noted that the irreversibility of cyclic slip implies fundamental fatigue mechanisms, which should rather be represented by a parameter depending on the actual loading and microstructure [32]. Slip transmission form the first grain to the neighbouring grains is considered by the use of sensor elements. These kinds of boundary elements are placed in the neighbouring grains at the intersection points between the slip band in grain 1 and the grain boundaries, representing the potential slip systems of the respective grains (see Fig. 8). During each calculation step, crack advance results in a decrease in $\Delta CTSD$ along the slip band in grain 1 and a stress increase at the sensor elements, respectively. As soon as a critical

Table 2
Cyclic Hall–Petch data for the different kinds of phase ($\alpha\gamma$) and grain ($\alpha\alpha$, $\gamma\gamma$) boundaries in duplex stainless steel (cf. [11]).

	$\gamma\gamma$	$\alpha\alpha$	$\alpha\gamma$	Duplex
Microstructural cyclic yield stress $\sigma_{c\gamma}$ (MPa)	137	198	–	196
Cyclic Hall–Petch constant $k_{c\gamma}$ (MPa$\sqrt{\text{mm}}$)	4.2	5.0	15.8	10.1

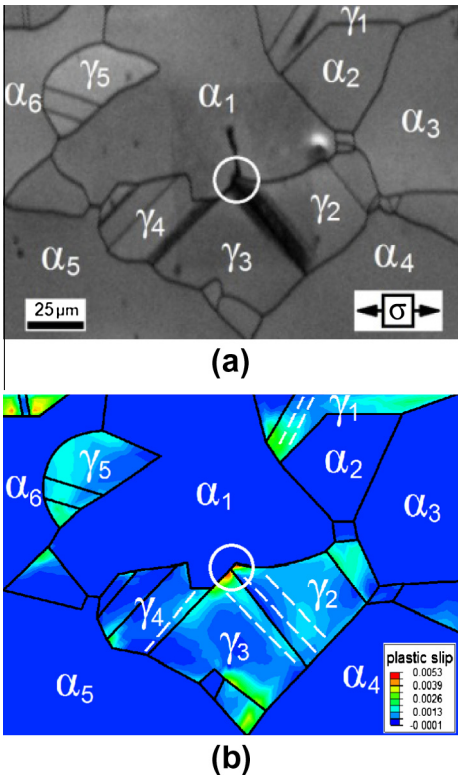

Fig. 7. Crack initiation at a ferrite–austenite grain boundary as a consequence of elastic/plastic anisotropy: (a) SEM micrograph of the fatigued surface of DSS: $\Delta\sigma/2 = 380$ MPa, 2,000,000 cycles, and (b) respective FEM simulation based on EBSD data and an elastic anisotropic/crystal plastic material model [9].

stress value is exceeded at one of the sensor elements, the respective slip band is meshed by a set of boundary elements and the displacement field is extended by one grain. Consequently, the fatigue crack and the plastic zones follow the given microstructure arrangement, while the barrier strength is implied in the use of sensor elements. Furthermore, slip along two alternating operating slip systems can be accounted for by measuring the stress distribution at the propagating crack tip [14].

For verification, the model was successfully applied to a variety of experimentally observed HCF and LCF fatigue cracks in the as-received and embrittled condition using the respective EBSD data and the crack geometries observed during fatigue experiments [8,21,29]. Since in LCF the tests are carried out under plastic strain control, the stress amplitude used for calculation was that attained during the saturation stage and corresponds to $\Delta\sigma/2 = 300$ MPa. Fig. 9a shows a calculated crack path in comparison with an experimentally observed crack. The start of the crack was defined according to the experimental result, i.e., the α/α grain boundary. According to the model, in grain #1 the crack grows on a single-slip (1 1 1) plane and after few cycles, an additional slip system is activated resulting in crack propagation on multiple slip bands. In the austenite grain #2 the crack grows by double slip operating systems with high Schmid factors 0.48 and 0.49, respectively. After several cycles the crack returns to single-slip propagation on the

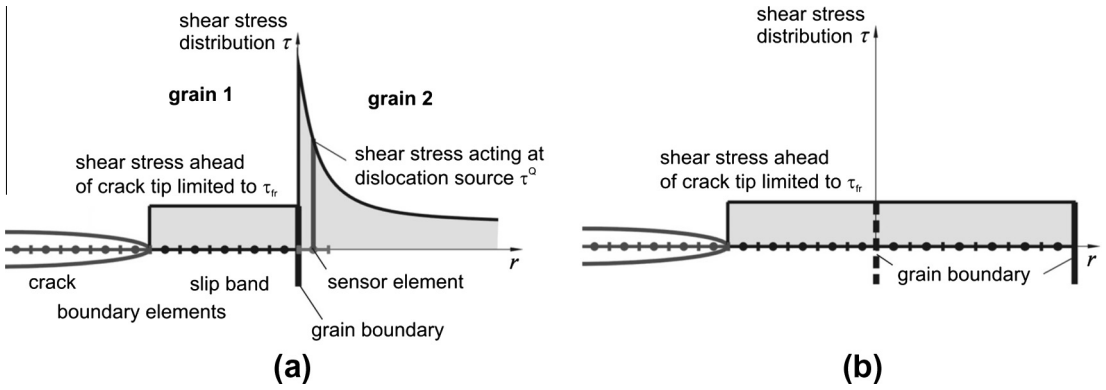

Fig. 8. Schematic representation of the boundary element modelling concept showing the stress distribution within the yield strip ahead of the crack tip: (a) plastic slip blocked by grain boundary, and (b) slip transmission to neighbouring grain.

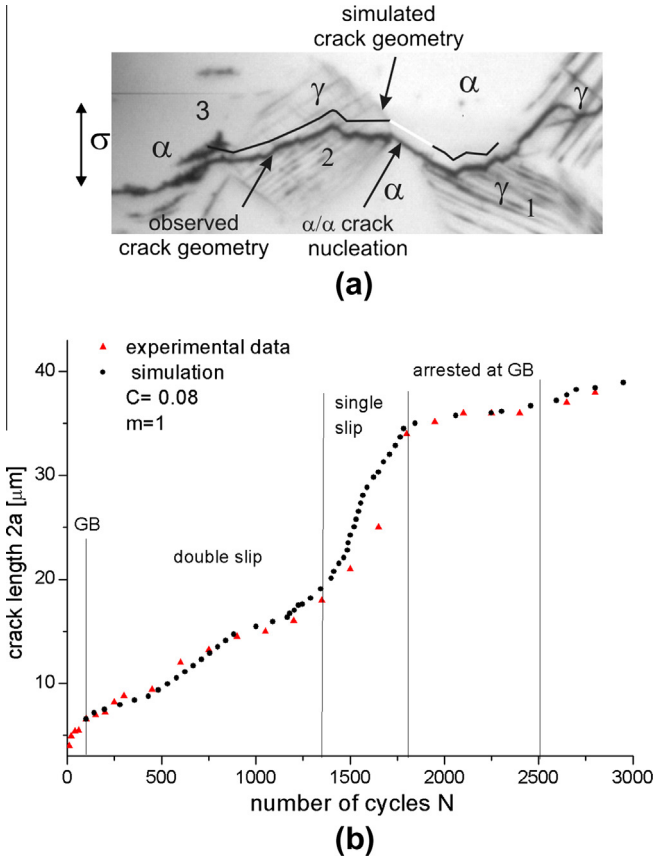

Fig. 9. (a) Scanning electron micrograph showing the crack path and the simulated crack path; and (b) comparison of the calculated and measured values of the crack lengths versus the number of cycles during LCF.

plane up to the phase boundary where it is arrested. Finally, the crack grows on a (112) plane in the ferritic grain #3. Therefore, the model agrees well with the behaviour of the real crack [28]. Fig. 9b shows the simulated crack length versus number of loading cycles in comparison with experimental data. A change in the crack propagation rate was observed when the crack path switched from double slip to single slip, increasing the crack propagation rate until the boundary phase was reached where the crack was arrested for several cycles. The predicted crack growth rate is in good agreement with the experimental data. The blocking of the slip bands at the grain boundaries as well as the retardation of the crack while approaching the boundary can be simulated.

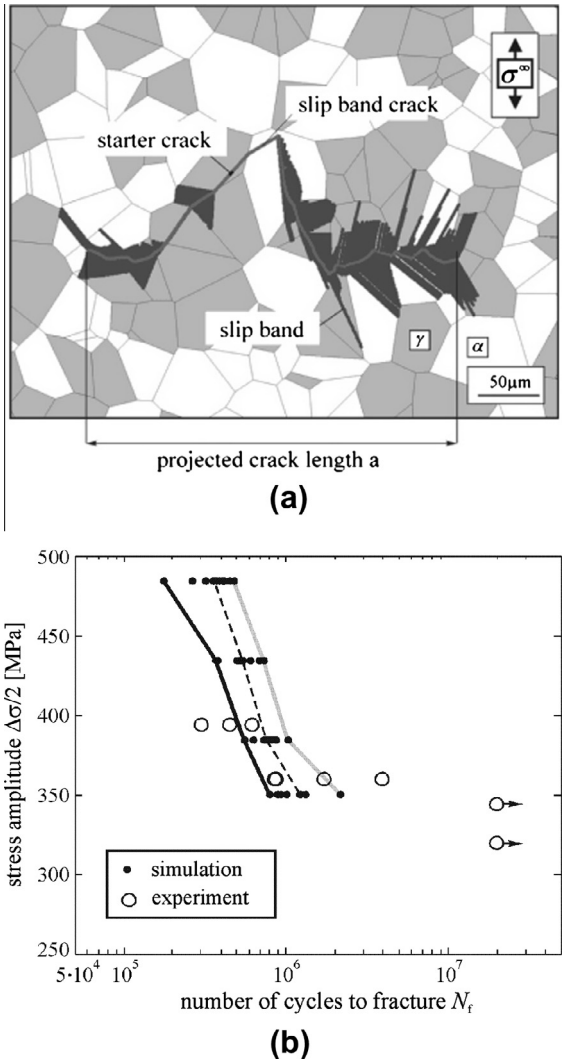

Fig. 10. Simulation of microcrack propagation: (a) calculated crack path and activated slip bands in a synthetic Voronoi microstructure and (b) respective S/N fatigue life data in comparison with experimental data [29].

Alternatively, the model can be applied to synthetic microstructures, e.g., generated by the Voronoi algorithm. Such a simulation of a crack propagating through a DSS microstructure is shown in Fig. 10a. To obtain the fatigue life, the simulations were stopped when a critical projected crack length of 1 mm (in a cylindrical

specimen of 7 mm diameter) was reached. For each of the four stress levels shown in the S/N Wöhler diagram in Fig. 10b only the fastest cracks of 100 simulations were used to derive the fatigue life taking into account that under real conditions many crack embryos are formed, but only one or two form the final crack. When all of the crack embryos are stopped completely by the barrier strength of phase and grain boundaries, the fatigue limit is reached [29].

The simulations are in reasonable agreement with the experimental data. In particular, the simulation results represent the scatter in the fatigue life, which increases with increasing number of cycles (and decreasing stress amplitude). As a conclusion, the scatter in fatigue life can be attributed to the probabilistic arrangement of the microstructure of the material, as it is outlined by the scheme in Fig. 1.

5. Conclusion

Research work on the short crack propagation behaviour of duplex stainless steel in the low-cycle (LCF), high-cycle (HCF), and in the very-high-cycle fatigue (VHCF) regime, revealed a strong dependence of the cyclic plasticity in the ferrite phase from the remote stress amplitude. While the fcc austenite grains show slip band formation even at very low stress amplitudes up to one billion of cycles, the stronger bcc ferrite grains exhibit dislocation patterning only under LCF loading conditions. Obviously, the dislocation networks in the ferrite promote transfer of the slip bands from the austenite grains. Under HCF and VHCF loading conditions, the ferrite phase contains only very few dislocations, giving rise to an increased barrier strength of the respective austenite-ferrite phase boundaries and, consequently, a higher fatigue life as compared to LCF loading. The fatigue life under HCF/VHCF loading conditions is determined by the initiation phase of technical cracks. During this phase, microstructurally short fatigue cracks strongly interact with grain and phase boundaries. For the situation that all barriers are sufficiently strong to block transmission of plasticity across grain and phase boundaries, duplex steel seems to exhibit a real fatigue limit. Furthermore, depending on the probabilistic arrangement of the material's microstructure, the fatigue life data exhibit a pronounced scatter. This was proven by a microstructure-based numerical short crack model.

Acknowledgments

The financial support by Deutsche Forschungsgemeinschaft DFG, Deutscher Akademischer Austauschdienst (DAAD) and Consejo Nacional de Investigaciones Científicas y Técnicas (CONICET Argentina) are gratefully acknowledged. Furthermore, the authors are grateful to Dr. MC Marinelli for the verification of the model in LCF.

References

[1] Alvarez-Armas I, Degallaix-Moreuil S, editors. Duplex stainless steels. London: ISTE/Wiley; 2009.
[2] Marinelli MC, Bartali Ahmed El, Signorelli JW, Evrard P, Aubin V, Alvarez-Armas I, et al. Activated slip systems and microcrack path in LCF of a duplex stainless steel. Mater Sci Eng A 2009;509:81–8.
[3] Serre I, Salazar D, Vogt J-B. Atomic force microscopy investigation of surface relief in individual phases of deformed duplex stainless steel. Mater Sci Eng A 2008;492:428–33.
[4] Vogt J-B, Salazar D, Serre I. Partition of cyclic plasticity in the 25Cr–7Ni–0.25N duplex stainless steel investigated by atomic force microscopy. In: Alvarez-Armas I, Degallaix-Moreuil S, editors. Duplex stainless steels. ISTE/WILEY; p. 275–300 [Chapter 8].
[5] Polák J, Zezulka P. Short crack growth and fatigue life in austenitic–ferritic duplex stainless steel. Fatigue Fract Eng Mater Struct 2005;28:923–35.
[6] Balbi M, Avalos M, El Bartali A, Alvarez-Armas I. Int J Fatigue 2009;31:2006–13.
[7] Polák J, Petrenec M, Man J, Obrtlik K. Initiation and short crack growth in austenitic–ferritic duplex steel – effect of positive mean stress. Fatigue Fract Eng Mater Struct 2012;35:257–68.
[8] Krupp U. Fatigue crack propagation in metals and alloys. Weinheim: Wiley VCH; 2007.
[9] Dönges B, Knobbe H, Christ H-J, Köster P, Fritzen C-P, Krupp U. Localization of crack initiation sites during fatigue of an austenitic–ferritic duplex steel in the high and very high-cycle fatigue (HCF/VHCF) regime. In: Proc. materials science and technology 2011 MS&T 11, Columbus, Ohio, USA.
[10] Krupp U, Giertler A, Marinelli MC, Knobbe H, Christ H-J, Köster P, Fritzen C-P, Hereñú S, Alvarez-Armas I. Efficiency of grain and phase boundaries as microstructural barriers during HCF and VHCF loading of austenitic–ferritic duplex steel. In: Proc. 5th int. conf. on VHCF, Berlin, Germany; 2011. p. 127.
[11] Krupp U, Düber O, Christ H-J, Künkler B, Schick A, Fritzen C-P. Application of the EBSD technique to describe the initiation and growth behaviour of microstructurally short fatigue cracks in a duplex steel. J Microsc 2004;213:313–20.
[12] Jha SK, Szczepanski SJ, Przybyla CP, Larsen JM. The hierarchy of fatigue mechanisms in the long-lifetime regime. In: Proc. 5th int. conf. on VHCF, Berlin; 2011. p. 505.
[13] Alvarez-Armas I, Krupp U, Balbi M, Herenu S, Marinelli MC, Knobbe H. Growth of short cracks during low and high cycle fatigue in a duplex stainless steel. Int J Fatigue 2012;41:95–100.
[14] Düber O, Künkler B, Krupp U, Christ H-J, Fritzen C-P. Experimental characterization and two-dimensional simulation of short-crack propagation in an austenitic–ferritic duplex steel. Int J Fatigue 2006;28:983–92.
[15] Alvarez-Armas I, Knobbe H, Marinelli MC, Balbi M, Hereñú S, Krupp U. Experimental characterization of short fatigue crack kinetics in an austeno-ferritic duplex steel. Proc Eng 2011;10:1491–6.
[16] Park KH, Lasalle JC, Schwartz LH. Mechanical properties of spinodally decomposed Fe–30 wt% Cr alloys: yield strength and aging embrittlement. Acta Metall 1985;33:205–11.
[17] Girones A, Llanes L, Anglada M, Mateo A. Cyclic deformation of superduplex stainless steels at intermediate temperatures. Metall Trans A, Phys 2006;37A:3519.
[18] Armas AF, Hereñú S, Alvarez-Armas I, Degallaix S, Condó A, Lovey F. The influence of temperature on the cyclic behavior of aged and unaged super duplex stainless steels. Mater Sci Eng A 2008;491:434–9.
[19] Hereñú S, Sennour M, Balbi M, Alvarez-Armas I, Thorel A, Armas AF. Influence of dislocation glide on the spinodal decomposition of fatigued duplex stainless steels. Mater Sci Eng A 2011;528:7636–40.
[20] Balbi M, Hereñú S, Proriol Serre I, Vogt J-B, Armas AF, Alvarez-Armas I. Initiation and growth of short cracks during cycling inan aged superduplex stainless steel. Key Eng Mater 2011;465:411–4.
[21] Marinelli MC, Krupp U, Kübbeler M, Hereñú S, Alvarez-Armas I. The effect of the embrittlement on the fatigue limit and crack propagation in a duplex stainless steel during high cycle fatigue. Eng Fract Mech 2013. http://dx.doi.org/10.1016/j.engfracmech.2013.03.034.
[22] Heinz A, Neumann P. Crack initiation during high-cycle fatigue of an austenitic steel. Acta Met Mater 1990;38:1933.
[23] Blochwitz C, Tirschler W. Twin boundaries as crack nucleation sites. Cryst Res Technol 2005;40:32.
[24] Krupp U, Knobbe H, Christ H-J, Köster P, Fritzen C-P. The significance of microstructural barriers during fatigue of a duplex steel in the high and very high-cycle fatigue (HCF/VHCF) regime. Int J Fatigue 2010;32:914–20.
[25] Tanaka K, Mura T. A dislocation model for fatigue crack initiation. J Appl Mech 1981;48:97–103.
[26] Chan KS. A microstructure-based fatigue crack initiation model. Met Mater Trans A 2003;34A:43–58.
[27] Düber O. Untersuchungen zum Ausbreitungsverhalten mikrostrukturell kurzer Ermüdungsrisse in zweiphasigen metallischen Werkstoffen am Beispiel eines austenitisch-ferritischen Edelstahls. VDI-Fortschritt-Berichte, Reihe 5, Nr. 730, VDI Verlag, Düsseldorf; 2007.
[28] Marinelli MC, Giertler A, Sahu JK, Hereñu S, Alvarez I, Krupp U. The effect of ferrite embrittlement in duplex steel on fatigue crack propagation from the low (LCF) to the very high cycle fatigue (VHCF) regime. In: 19th European conference on fracture. European structural integrity society ESIS, Kasan, Russia; 2012
[29] Künkler B. Mechanismenorientierte Lebensdauervorhersage unter Berücksichtigung der Mikrostruktur. VDI-Fortschritt-Berichte, Reihe 18, Nr. 312, VDI Verlag, Düsseldorf, Germany; 2007.
[30] Künkler B, Düber O, Köster P, Krupp U, Fritzen C-P, Christ H-J. Modelling of the transition from stage I to stage II short crack propagation. Eng Fract Mech 2008;75:715–25.
[31] Sahu J. Effect of 475 °C embrittlement on the fatigue behaviour of duplex stainless steel. PhD thesis, University of Siegen, Germany; 2008.
[32] Shyam A, Milligan WW. A model for slip irreversibility, and its effect on the fatigue crack propagation threshold in a nickel-base superalloy. Acta Mater 2005;53:835–44.